Science
AAAS

Radiationless Electromagnetic Interference: Evanescent-Field Lenses and Perfect Focusing

R. Merlin, *et al.*

Science **317**, 927 (2007);
DOI: 10.1126/science.1143884

Radiationless Electromagnetic Interference: Evanescent-Field Lenses and Perfect Focusing

R. Merlin

Diffraction restricts the ability of most electromagnetic devices to image or selectively target objects smaller than the wavelength. We describe planar subwavelength structures capable of focusing well beyond the diffraction limit, operating at arbitrary frequencies. The structure design, related to that of Fresnel plates, forces the input field to converge to a spot on the focal plane. However, unlike the diffraction-limited zone plates, for which focusing results from the interference of traveling waves, the subwavelength plates control the near field and, as such, their superlensing properties originate from a static form of interference. Practical implementations of these plates hold promise for near-field data storage, noncontact sensing, imaging, and nanolithography applications.

The closely related problems of electromagnetic imaging and focusing beyond Abbe's diffraction limit, set by ~λ/*n*, where λ is the vacuum wavelength and *n* is the refractive index (*1*), have received considerable attention in the past decade, motivated in part by optical studies using subwavelength apertures to probe the near field (*2*) and related work at microwave frequencies (*3*). Various schemes have been developed to improve the resolution, involving, for example, sharp tips (*4*, *5*), coherent control (*6*) and far-field time-reversal mirrors (*7*), and values as small as ~λ/100 have been reported for the THz range (*8*). Subwavelength focusing necessarily involves the evanescent components of the field, that is, the near field. Because of this, standard interference techniques or geometrical optics methods do not apply. More recently, negative refraction has emerged as a topic of interest to near-field studies (*9*, *10*), following proposals of perfect lensing (*11*–*14*) and the subsequent experimental verification of negative refraction at microwave frequencies (*15*, *16*) and imaging beyond Abbe's limit with negative-permittivity slabs (*17*, *18*). In this work, an approach to subwavelength focusing is described that uses patterned, planar structures to induce convergence of the near field. The focusing effect described is reminiscent of, but the physics is substantially different from, that of both negative refraction slabs and Fresnel zone plates (*19*).

Let F be one of the cartesian components of the electric (**E**) or the magnetic (**H**) field , and assume that all the field sources are monochromatic, with time dependence given by $e^{-i\omega t}$ (ω is the angular frequency), and that they lie to the left of a particular plane, defined as $z = 0$. Then, for $z \geq 0$, F satisfies the Helmholtz equation $\nabla^2 F + k^2 F = 0$ and can thus be expressed in the angular-spectrum-representation form (*20*, *21*)

$$F(x,y,z_\alpha) = \frac{1}{4\pi^2}\int_{-\infty}^{+\infty}\!\!\iiint F(x',y',z_\beta) \times e^{i[q_x(x-x')+q_y(y-y')+\kappa(z_\alpha-z_\beta)]}dx'dy'dq_xdq_y \quad (1)$$

providing an exact relationship between the solution to the wave equation in two arbitrary planes, parallel to each other, $z = z_\alpha > 0$ and $z = z_\beta > 0$. Here, $k = 2\pi/\lambda$ and

$$\kappa = \begin{cases} i\left|(q_x^2+q_y^2-k^2)^{1/2}\right| & q_x^2+q_y^2 \geq k^2 \\ \left|(k^2-q_x^2-q_y^2)^{1/2}\right| & q_x^2+q_y^2 < k^2 \end{cases} \quad (2)$$

With the sources located in the half-space $z < 0$, the choice of signs in Eq. 2 is dictated by the requirements that the homogeneous and inhomogeneous (or evanescent) solutions to the wave equation must travel and decay in the positive z direction, respectively.

According to Eq. 1, the field in the region $z \geq 0$ is determined by the boundary values $F(x,y,0)$. Hence, the question of focusing (for both the subwavelength and the conventional, diffraction-limited cases) becomes that of identifying the sources needed to generate the field profile at $z = 0$ that converges to a spot of a predetermined size at the focal plane, $z = f$. Although the angular-spectrum representation shows that $F(x,y,0)$ is, in turn, uniquely determined by the focal-plane values, $F(x,y,f)$, the answer to the focusing problem is not unique, and the search for the optimal solution is not trivial, because "focal spot" is, at best, an electromagnetically vague concept. The difficulty here is that the wrong choice of $F(x,y,f)$ may result in a field that is unsuitable for applications, that diverges, or that does not exist (everywhere in a region or at certain points), or in a boundary field that is difficult to implement in practice. In our approach, $F(x,y,0)$ is defined by the transmission properties of subwavelength-patterned planar structures that behave, in some sense, like the evanescent-wave counterparts to Fresnel's zone plates (*19*). Similar to the latter structures, the waves exit our plates in a pattern set by the plate design, which forces them to converge to a spot on the focal plane, as prescribed by Eq. 1. Unlike the Fresnel plates, which rely on interference involving radiative components of the field, and are thus subjected to Abbe's constraint, our plates affect primarily the evanescent waves leading to interference effects that are electrostatic or magnetostatic in nature and, as a result, the spot size can be arbitrarily small. As with other near-field effects, our plates' ability to focus at large distances is severely limited by the exponential decay of the near field which, in practical applications, constrains the focal length to dimensions much smaller than λ.

The proposed plates can be tailored to give subwavelength focal patterns of various types and symmetries. We concentrate on two key geometries displaying cylindrical and azimuthal symmetry. In the cylindrical or two-dimensional case, $\partial F / \partial x = 0$, the perfect focus is a line, and Eq. 1 becomes

$$F(y,z_\alpha) = \frac{1}{2\pi}\int_{-\infty}^{+\infty}\!\!\iint F(y',z_\beta) \times e^{i[q(y-y')+\kappa(z_\alpha-z_\beta)]}dy'dq \quad (3)$$

where $\kappa(q)$ is given by Eq. 2 with $q_x^2 + q_y^2 \rightarrow q^2$. For electromagnetic fields propagating in the $+z$ direction that have azimuthal symmetry, such as the axicon (*22*) and Bessel beams (*23*), the tangential ϕ component of the electric field, as well as the z and radial ρ component of **H** vanish, whereas the nonzero components $\Psi = H_\phi$ or E_ρ obey

$$\Psi(\rho,z_\alpha) = \int_{-\infty}^{+\infty}\!\!\iint \Psi(\rho',z_\beta)J_1(q\rho')J_1(q\rho) \times e^{i\kappa(z_\alpha-z_\beta)}\rho'd\rho'qdq \quad (4)$$

Replacing the Bessel function J_1 by J_0, one obtains the corresponding expression for E_z. Note that $e^{iq_0y}\exp[i\kappa(q_0)z]$ and $J_1(q_0\rho)\exp[i\kappa(q_0)z]$ are, respectively, solutions of Eqs. 3 and 4 for arbitrary q_0 that become evanescent modes for $|q_0| > k$. For $|q_0| < k$, the corresponding fields are the well-known diffraction-free plane waves and Bessel beams. These states and, more generally, source-free electromagnetic fields with components of the form $f_{q_0}(\boldsymbol{\rho})\exp[i\kappa(q_0)z]$, where **ρ** is a vector normal to the z axis, play a crucial role in near-field lensing.

Our approach to subwavelength focusing relies on a property of the near field that, to the best of our knowledge, has not been considered before. Assume that $f_{q_0}\exp[i\kappa(q_0)z]$ is part of a full solution to Maxwell's equations and that a

Department of Physics, The University of Michigan, Ann Arbor, MI 48109–1040, USA. Email: merlin@umich.edu

certain field component (cartesian or otherwise) at the source plane, $z = 0$, is of the form $M(\boldsymbol{\rho}) \times f_{q_0}(\boldsymbol{\rho})$ where M is a modulation function, which is characterized by the length scale $L \gtrsim \ell \equiv 2\pi/|q_0|$ and satisfies the requirements specified below. Then, it can be shown for $|q_0| >> k$ that the field converges to a focal spot of resolution defined by ℓ, after propagating through a distance of order L. This effect is illustrated for both the two-dimensional and azimuthally symmetric case in Fig. 1. The basic concepts of near-field lensing are best understood in the cylindrical geometry. In Eq. 3, take $F(y,0) = M(y)e^{iq_0 y}$ and integrate to calculate $F(y,z)$. For $|q_0| >> k$, the relevant states are evanescent waves. We can therefore approximate $\kappa(q) \approx i|q|$ so that $F(y,z) \approx \iint e^{iqy} e^{-|q|z} M(y') e^{i(q_0 - q)y'} dy' dq/2\pi$ (in this approximation, F is harmonic, i.e., $\nabla^2 F \approx 0$, for arbitrary M). Lensing occurs for a wide variety of modulation functions. Mathematically, a sufficient condition for focusing is that M should have one or more poles in the complex plane with nonzero imaginary components. To prove this, we assume that $M(y)$ is a real and even function, with poles at $\pm iL$. Performing a simple integration we obtain, for $q_0 > 0$, $F(y,z) \propto Le^{-q_0 L} g(y,z)$ where

$$g(y,z) = \left[\frac{e^{q_0(iy+L-z)} - 1}{iy + L - z} + \frac{(iy + L + z)e^{q_0(iy+L-z)} + (-iy + L + z)}{y^2 + (z+L)^2} \right] \quad (5)$$

As anticipated, the expression inside the brackets leads to focusing at $z = L$ such that, for $L >> \ell$, $|F(y,L)| \propto Le^{-q_0 L} |\sin(q_0 y/2)/y|$ (note that the singularity at $z = L$ and $y = 0$ is removable and that the second term gives a small correction of order ℓ/L to the resolution). Because there are no phases associated with evanescent waves, it should come as a surprise that the lensing process shows telltale signs of conventional interference, particularly in the way the waves contributing to Eq. 3 add up constructively and destructively at the focal plane. Because it involves nonradiative modes, we will refer to this unconventional form of focusing as radiationless interference.

Figure 1A shows plots of $|F(y,z)|^2$, obtained from Eq. 3, for $f_{q_0} = e^{iq_0 y}$ and $M = (1 + y^2/L^2)^{-1}$. This form of M is the simplest one for an even function with poles at $y = \pm iL$. The calculations are consistent with Eq. 5 and support our contention that, for $L \gtrsim \ell$, the focal length and the resolution are determined, independently, by the modulation length, L, and the length scale of the unperturbed field component, ℓ. As shown in Fig. 1B, the modulated azimuthally symmetric field (ringlike focus) exhibits a similar effect.

Although our study so far has been limited to simple poles located in the imaginary axis, it can be shown that (i) focusing can also be attained with higher-order poles, (ii) modulation functions with multiple poles give multiple foci, and (iii) the real and imaginary part of a given pole determine, respectively, the off-axis position of the focal spot and the corresponding focal length. Within this context, it is of interest to apply our analysis to a negative-refraction slab that exhibits perfect focusing at $n = -1$ (*11*). For $|1 + n| << 1$ and a source consisting of a line of dipoles, the expression for the field is known analytically (*13*, *14*). In particular, if the slab thickness is d and the source is at a distance $d/2$ from the nearest slab surface and, therefore, its image is at $d/2$ from the other surface (*11*), the evanescent field at the exit side of the slab can be written as $M(y)e^{iq_0 y}$ where

$$M(y) \propto \frac{\cosh(\pi y/2d) - i \sinh(\pi y/2d)}{\cosh(\pi y/2d) + i \sinh(\pi y/2d)} \quad (6)$$

and $q_0 = -\ln|1 + n| / d$ (*14*). As expected, M exhibits a pole at $y = id/2$, reflecting the image location and, moreover, the expression for q_0 is in perfect agreement with the known slab resolution (*13*, *14*, *24*). Because M has an infinite number of additional poles at $y = i(d/2 + 2pd)$, where $p > 0$ is an integer, a near-perfect slab will exhibit not just one, but an infinite number of images for which the intensity decays exponentially with p. These additional images are due to multiple reflections arising from the slight impedance mismatch at the slab-vacuum interfaces.

For the two-dimensional geometry, the above results can be trivially extended from the simple sinusoidal to the general case of a periodic field $P_\ell(y)$, of period ℓ. It is apparent that, for values at the source plane given by $F(y,0) = M(y)P_\ell(y)$, the field will converge at $z = L$ to a focal spot of size $\sim\ell$. This suggests the path for a practical implementation of cylindrical near-field lensing. As a periodic field can be simply realized by letting a plane wave go through an array of periodically placed slits or ribbons, it is clear that a

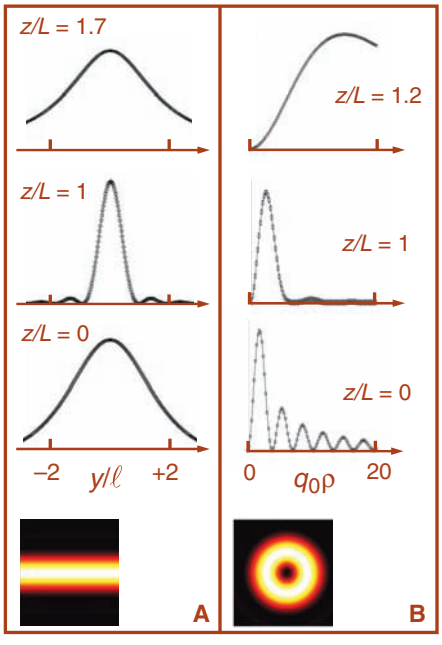

Fig. 1. Subwavelength focusing. (**A**) Two-dimensional case: $|F(y,z)|^2$ versus y/ℓ from Eq. 3 where $F(y,0) \propto e^{iq_0 y}/(1 + y^2/L^2)$ and $L/\ell = 2.5$. (**B**) Azimuthally symmetric geometry: $|\Psi(\rho,z)|^2$ versus $q_0\rho$ from Eq. 4 where $\Psi(\rho,0) \propto J_1(q_0\rho)/(1 + \rho^2/L^2)$ and $L/\ell = 8$. The contour plots show the focal line (A) and ring (B) at $z = L$.

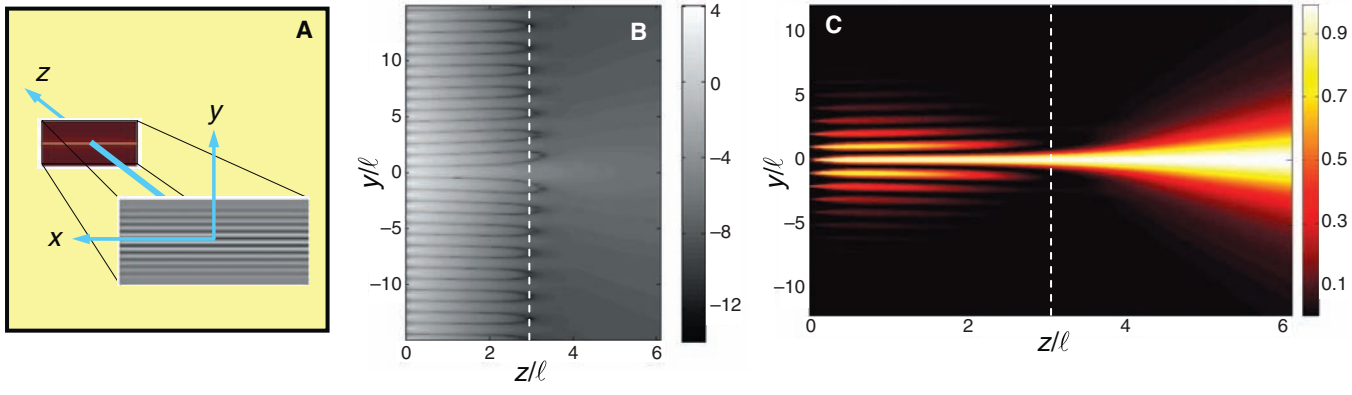

Fig. 2. Radiationless interference. (**A**) Schematic showing a subwavelength plate, represented as a modulated array of linear current sources at $z = 0$ and the plane showing the focal line. $L/\ell = 3$; see Eq. 7. (**B**) Contour plot of $\ln|H_y|$. (**C**) Contour plot of $|H_y(z,y) / H_y(z,0)|^2$. The dashed white line at $z = L$ denotes the focal plane.

field of the form $M(y)P_\ell(y)$ can be obtained by introducing a slowly varying modulation in, say, the width or the properties of the material of which an element is made. Similarly, in the case of azimuthal symmetry, a Bessel beam can be used together with a set of concentric rings of properly modulated width placed at radii satisfying $J_1(q_0\rho) = 0$. The technology for manufacturing plates of this kind for microwave applications has been available for quite some time, whereas nanofabrication methods involving, for example, electron and focused ion beam lithography, can be used for the infrared and optical range. An important consideration in the design of a near-field plate is to avoid as much as possible the presence of terms giving a background that could overwhelm the sharp features of the field. An example of background-free focusing is shown in Fig. 2. These results are for the diffraction of a plane wave by a set of ribbons of very narrow width $<< \ell$ and parameters such that the total current density is $\mathbf{j} = (j_x,0,0)$ where

$$j_x \propto \delta(z) \sum_{s=-\infty}^{\infty} \frac{(-1)^s \delta(y - s\ell)}{(1 + s^2\ell^2/L^2)} \qquad (7)$$

(the incident electric field is parallel to the cylindrical axis). Such an array of currents, with the sign varying from one element to the next, can be realized at infrared and optical frequencies by alternating material with positive and negative permittivity and, in the microwave regime, by using a set of interchanging capacitive and inductive elements. Figure 2B shows a contour plot of the y component of the diffracted magnetic field (logarithmic scale). These results are similar to those reported for negative-index slabs (*14*, *25*), thereby revealing the close relationship between the two phenomena (*26*). Finally, to help ascertain the origin of radiationless interference, we show in Fig. 2C a linear plot of the field intensity, normalized to its largest value at a given z. Reflecting a property of the zeros of H_y, the figure clearly shows behavior reminiscent of beam coupling in that the diffraction of the beam produced by a particular current source is prevented by the presence of its neighbors. It is only after the intensity of its neighbors has decreased a sufficient amount that the central beam is allowed to spread, and the point at which this happens determines the focal length.

References and Notes

1. E. Abbe, *Arch. Mikrosk. Anat.* **9**, 413 (1873).
2. E. Betzig, J. K. Trautman, *Science* **257**, 189 (1992).
3. A. Tselev *et al.*, *Rev. Sci. Instrum.* **74**, 3167 (2003).
4. F. Zenhausern, Y. Martin, H. K. Wickramasinghe, *Science* **269**, 1083 (1995).
5. R. Hillenbrand, T. Taubner, F. Keilmann, *Nature* **418**, 159 (2002).
6. M. I. Stockman, S. V. Faleev, D. J. Bergman, *Phys. Rev. Lett.* **88**, 067402 (2002).
7. G. Lerosey, J. de Rosny, A. Tourin, M. Fink, *Science* **315**, 1120 (2007).
8. P. C. M. Planken, N. C. J. van der Valk, *Opt. Lett.* **29**, 2306 (2004).
9. D. R. Smith, J. B. Pendry, M. C. K. Wiltshire, *Science* **305**, 788 (2004).
10. D. R. Smith, *Science* **308**, 502 (2005).
11. J. B. Pendry, *Phys. Rev. Lett.* **85**, 3966 (2000).
12. N. A. P. Nicorovici, R. C. McPhedran, G. W. Milton, *Phys. Rev. B* **49**, 8479 (1994).
13. G. W. Milton, N. A. P. Nicorovici, R. C. McPhedran, V. A. Podolskiy, *Proc. R. Soc. London Ser. A* **461**, 3999 (2005).
14. R. Merlin, *Appl. Phys. Lett.* **84**, 1290 (2004).
15. R. Shelby, D. R. Smith, S. Schultz, *Science* **292**, 77 (2001).
16. A. Grbic, G. V. Eleftheriades, *Phys. Rev. Lett.* **92**, 117403 (2004).
17. N. Fang, H. Lee, C. Sun, X. Zhang, *Science* **308**, 534 (2005).
18. T. Taubner, D. Korobkin, Y. Urzhumov, G. Shvets, R. Hillenbrandt, *Science* **313**, 1595 (2006).
19. E. Hecht, *Optics* (Addison Wesley, San Francisco, 2002).
20. J. A. Stratton, *Electromagnetic Theory* (McGraw-Hill, New York, 1941).
21. P. C. Clemmow, *The Plane Wave Spectrum Representation of Electromagnetic Fields* (Pergamon, Oxford, 1966).
22. J. H. McLeod, *J. Opt. Soc. Am.* **44**, 592 (1954).
23. J. Durnin, J. J. Miceli Jr., J. H. Eberly, *Phys. Rev. Lett.* **58**, 1499 (1987).
24. D. R. Smith *et al.*, *Appl. Phys. Lett.* **82**, 1506 (2003).
25. G. Shvets, *Phys. Rev. B* **67**, 035109 (2003).

26. We emphasize that, although our plates and negative-index slabs create comparable field distributions, the physical origins are very different in that the plates transform, propagating into evanescent modes, whereas the slabs amplify the near field.

27. The author acknowledges discussions with A. Grbic. This work was supported by the Air Force Office of Scientific Research under contract FA 9550-06-01-0279 through the Multidisciplinary University Research Initiative Program.

16 April 2007; accepted 27 June 2007
Published online 12 July 2007;
10.1126/science.1143884
Include this information when citing this paper.

Coherent Optical Spectroscopy of a Strongly Driven Quantum Dot

Xiaodong Xu,[1] Bo Sun,[1] Paul R. Berman,[1] Duncan G. Steel,[1]* Allan S. Bracker,[2] Dan Gammon,[2] L. J. Sham[3]

Quantum dots are typically formed from large groupings of atoms and thus may be expected to have appreciable many-body behavior under intense optical excitation. Nonetheless, they are known to exhibit discrete energy levels due to quantum confinement effects. We show that, like single-atom or single-molecule two- and three-level quantum systems, single semiconductor quantum dots can also exhibit interference phenomena when driven simultaneously by two optical fields. Probe absorption spectra are obtained that exhibit Autler-Townes splitting when the optical fields drive coupled transitions and complex Mollow-related structure, including gain without population inversion, when they drive the same transition. Our results open the way for the demonstration of numerous quantum level–based applications, such as quantum dot lasers, optical modulators, and quantum logic devices.

The quantum optoelectronic properties of semiconductor quantum dots (QDs) have featured prominently in numerous proposals, including quantum computing, single-photon sources, and quantum repeaters (*1*–*3*). QDs are particularly attractive for these applications because they behave in many ways as simple stationary atomic or molecular systems (*4*) with discrete states where the electron-hole pair can be treated as a well-defined composite-particle state (*5*).

Whereas strong optical excitation of a semiconductor creates a many-body problem because of the extended nature of the wave function (*6*), confinement of the wave function in QDs leads to strong energy-level shifts between one exciton and two or more exciton states, enabling the system to be considered as a relatively simple few-level problem. The strong-field excitation regime of the transition from the ground state to an excited state such as the exciton, a Coulomb bound electron-hole pair, is then defined by $\Omega_R >> 2\gamma$ where the Rabi frequency $\Omega_R = \frac{\mu E}{h}$, γ is a transition linewidth (full width at half-maximum, in Hz), μ is the transition dipole moment, and E is the amplitude of the optical electric field. For time scales less than γ^{-1}, strong excitation leads to Rabi oscillations (*7*–*10*) in time. The effect of vacuum Rabi splitting (*11*) has also been observed in a single QD embedded in a nanocavity (*12*–*14*).

Under strong continuous wave (CW) narrowband resonant optical excitation of a simple atomic system, the fluorescence emission spectrum, which is a narrow emission line at low power (the emission width is the laser bandwidth), consists of three peaks referred to as the Mollow triplet (*15*). A simple picture of the origin of this emission pattern is understood from a dressed-atom picture (*16*). Figure 1B shows the dressed-state picture with fully quantized atom-field states, when the driving-field frequency ω is equal to the electronic frequency ω_0. In this limit,

[1]The H. M. Randall Laboratory of Physics, The University of Michigan, Ann Arbor, MI 48109, USA. [2]The Naval Research Laboratory, Washington, DC 20375, USA. [3]Department of Physics, University of California–San Diego, La Jolla, CA 92093, USA.

*To whom correspondence should be addressed. E-mail: dst@umich.edu